Contact line behavior on nanoporous alumina surfaces

Vincent Raspal, Christophe Massard, Roshan Bokalawela, Matthew Johnson, Komla Oscar Awitor

Surface Innovations

Contact line behavior on nanoporous alumina surfaces
Raspal, Massard, Bokalawela, Johnson and Awitor

ice | science

http://dx.doi.org/10.1680/si.13.00011
Research Article
Received 10/05/2013 Accepted 28/06/2013
Published online 02/07/2013
Keywords: adhesion/alumina nanoporous surfaces/contact angle/contact angle hysteresis/contact line pinning/contact line thickness/nanostructures

ice Institution of Civil Engineers
publishing

Contact line behavior on nanoporous alumina surfaces

1 **Vincent Raspal** MD
C-BIOSENSS–EA 4676, Clermont Université, Université d'Auvergne, Clermont-Ferrand, France

2 **Christophe Massard** PhD
C-BIOSENSS–EA 4676, Clermont Université, Université d'Auvergne, Clermont-Ferrand, France

3 **Roshan S. P. Bokalawela** PhD
Department of Physics and astronomy, Nielsen Hall, University of Oklahoma, Norman, OK, USA

4 **Matthew B. Johnson** PhD
Department of Physics and astronomy, Nielsen Hall, University of Oklahoma, Norman, OK, USA

5 **Komla O. Awitor** PhD*
C-BIOSENSS–EA 4676, Clermont Université, Université d'Auvergne, Clermont-Ferrand, France

The aim of this study is to describe the behavior and the thickness of a three-phase system contact line on nanoporous alumina surfaces based on wetting hysteresis measurements. The nanoporous alumina templates were fabricated by anodization of aluminum foil in an oxalic or sulfuric acid solution. The oxide film consists of a well-ordered hexagonal array of pores with uniform diameter. The morphology was controlled by varying the pore diameter, depth and spacing. The wetting behavior of the nanoporous alumina templates was investigated using advancing and receding contact angle measurements carried out by varying the volume of the water droplets used. The surfaces showed a large hysteresis, with a receding contact angle always equal to zero making them strongly adhesive despite their hydrophobicity. Comparing linear and areal models indicates that the contact line thickness is negligible compared with the size of the nanopores. Contact line pinning highlights the role of the surface shape around the pores in the marked adhesive behavior of our templates.

1. Introduction

Nanoporous alumina templates consist of well-ordered arrays of pores, where the pore diameter, depth and spacing distance can be accurately varied. Such templates are an ideal system for measuring and modeling the effect of surface roughness on the wettability of nanostructured materials, leading to a more fundamental understanding of their wetting properties. In this study, the authors use a cost-effective process to fabricate alumina templates that allow us to tailor their wettability. The template morphology was characterized using scanning electron microscopy. The wetting behavior was studied by measuring the advancing and receding contact angles of water droplets. The method used was changing the drop volume with a computer-monitored syringe. The equilibrium contact angles for different liquids on nanoporous alumina templates have already been studied.[1]

The contact angle hysteresis can prevent a liquid drop from rolling off a tilted support. The concept of adhesion is derived from the hysteresis because contact angle hysteresis is directly related to the driving force of a liquid drop.[2] Hysteresis is also an obstacle in the measurement of equilibrium contact angles and has been reported for a long time. The Gibbs energy curves have been used to show metastable configurations that exist for real, inhomogenous and/or rough solid surfaces. Hysteresis has been studied experimentally for the last few decades. For example, Johnson and Dettre studied the evolution of hysteresis with increasing surface roughness.[3] Choi *et al.* focused on the wetting hysteresis of anisotropic microtextured surfaces,[4] pointing out that advancing and receding contact angles are ruled by a differential structure parameter that reflects the contact line's strong influence in advancing and receding processes. Nanoscale topography is likely to challenge these rules. Very few

*Corresponding author e-mail address: komla.awitor@udamail.fr

studies dealing with the wettability of nanotextured surfaces have been carried out.[5,6] Different wettability behaviors have been reported on nanostructured surfaces with different patterns, degree of regularity, materials used and their physical and chemical post-treatments.[7–11] Nanostructured materials and their associated hysteresis remain a good way to investigate, and ultimately to control, what happens at the nanoscale, especially at the three-phase contact line. The physics governing the behavior of this line is important for understanding the surface wetting mechanisms in general.

In this study, the authors describe the behavior and the thickness of the three-phase contact line on various nanoporous alumina surfaces. Wetting hysteresis is a good experimental base for a theoretical study, because it is affected by what happens at the level of the contact line. The nanoporous alumina templates were fabricated by anodization of aluminum foil either in an oxalic or in a sulfuric acid solution. Scanning electron microscopy was used to characterize the morphology of the surfaces. The wetting behavior of the nanoporous alumina templates was investigated using advancing and receding contact angle measurements carried out by increasing and decreasing the volume of water droplets.

2. Experimental section

2.1 Fabrication of nanoporous alumina templates

The nanoporous alumina templates were fabricated using a two-step anodization process on a pure (99·999%) aluminum foil, as described in detail elsewhere.[12,13] The two electrolytes used were 0·3-M oxalic and 0·3-M sulfuric acid solutions. First, the 0·25-mm thick aluminum foil was anodized in the acid solution at 3°C and at a potential E_0 that depends on the electrolyte used. The duration of this step was at least 17 h resulting in the growth of a thick porous oxide layer. The resulting nanoporous alumina film was then chemically stripped from the aluminum foil, and a secondary anodization was performed with the same solution, at the same temperature and voltage as in the first step. The duration of the second step is critical because it sets the thickness, H, of the final anodic oxide film (pore depth). Using this two-step procedure, good pore ordering was obtained over micrometer-sized regions. As-grown pore radii can be increased by chemical etching, without a noticeable change in the film thickness. This pore widening is linear in time with the diameters increasing about 6·6 nm per hour. The final pore diameters are denoted as d_p. The center-to-center distance between the pores, D, was set by the electrolyte used and voltage applied. Twenty-four different nanoporous samples were used. Their characteristics are summarized in Table 1. The acronyms OAAO and SAAO refer to oxalic and sulfuric anodic aluminum oxide, respectively.

A flat and smooth alumina surface was also prepared to serve as the reference sample. The authors used the same process as for OAAO templates, but with only one 30-s anodization. This corresponds to the time required to form the initial homogeneous smooth oxide layer. The sample produced was poreless with an oxide layer about 10-nm thick.

2.2. Topographic characterization

Characterization of the surface topography of the alumina samples was performed using a Zeiss Supra 55 VP scanning electron microscope (SEM) with secondary electron and in-lens detector. The accelerating voltage and the working distance were 3 kV and 4 mm, respectively.

2.3 Contact angle measurements

After the nanoporous samples were fabricated, the samples were thoroughly cleaned. Without careful cleaning, the contact angle measurements were not repeatable. Our cleaning procedure consisted of a 5-min ultrasonic bath in trichloroethylene, acetone, methanol and deionized water. Finally, the sample was blown dry with dry nitrogen. After this cleaning process, contact angle measurements were consistent – repeatable for different places on a sample and for different elapsed times.

The contact angle measurements were made using a contact angle goniometer with a drop-shape analysis system (Easy Drop, Kruss,

Electrolyte	E_0 (V)	D (nm)	H (nm)	d_p (nm)	Series
Oxalic acid				25 50 70 80	
			200		O200
	40	100	400	12 OAAO samples	O400
			800		O800
Sulfuric acid				20 25 30 40	
			200		S200
	25	65	400	12 SAAO samples	S400
			800		S800

OAAO, oxalic anodic aluminum oxide; SAAO, sulfuric anodic aluminum oxide.

Table 1. Experimental parameters used for the nanoporous samples fabrication – morphology indicators of these samples.

Hamburg, Germany). For these measurements, a 1-µl deionized water sessile droplet was placed on a sample, under ambient conditions, with a computer-controlled syringe. The measurement was monitored with a video capture system. First, the droplet volume was increased by adding deionized water at a rate of 10 µl/min. The droplet's evolution was recorded by the camera for about 10–15 s. This led to a maximum volume less than 4 µl. Immediately after this, the water was withdrawn at the same rate. The measurement took less than 1 min, any effect of water evaporation on drop shape was excluded. Later, the images, captured during these two steps, were analyzed using a droplet profile fitting method to determine the advancing and receding contact angles.

3. Results and discussions

3.1 The nanoporous templates

Figure 1(a) shows a top-down SEM image of a typical nanoporous alumina template (OAAO; d_p = 25 nm). This image indicates pore regularity with good hexagonal order. Figure 1(b) shows an oblique-angle view from which the template thickness was measured (H = 400 nm in this case).

A total of 25 different alumina surfaces were used. The first sample is a flat, smooth OAAO surface, while the others are surfaces with increasing pore radius obtained using longer pore-widening times. Figure 1(c) shows an optical view of three SAAO samples with a pore diameter of 30 nm and thickness of 200, 400 and 800 nm. The interference colors observed are evidence of the variation of the pore depth, H.

3.2 The contact angles

Figure 2 shows four examples of contact angle measurements on top of various surfaces. The advancing contact angles of the samples are displayed in Table 2. Irrespective of the series studied (Sxxx or Oxxx), the advancing angle increases monotonically with the pore diameter, d_p. The rate of this increase is greater for SAAO samples. The main difference between OAAO and SAAO samples is the distance between two adjacent pores, D. A second observation is that the pore depth does not influence the advancing contact angle (i.e. the values in a column are close to each other). This can also be observed in Figure 3, in which contact angle versus pore diameter is plotted. For each value of d_p, the points of the Sxxx and the Oxxx series are close together. For clarity, the series are framed by a dashed rectangle (oval) for the Sxxx (Oxxx) series. In addition, there is no tendency for different depths within a series to be consistently higher or lower than one another. For these reasons, the authors chose to calculate the mean value of the advancing contact angle, $\langle\theta_A\rangle$, for each diameter and each substrate (Table 2). In the rest of the article, the expression 'advancing contact angle' and the symbol 'θ_A' will actually refer to the 'mean value of the apparent advancing contact angle' and to the symbol '$\langle\theta_A\rangle$'. Table 2 also presents the advancing contact angle on the flat and smooth OAAO surface.

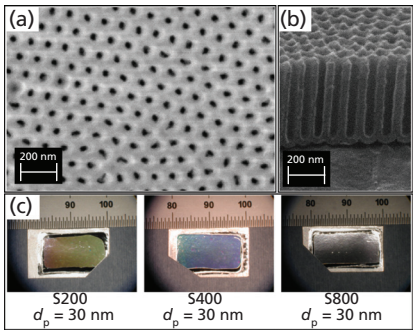

Figure 1. Top view shows the SEM images of a nanoporous alumina template from the O400 series with d_p = 25 nm (as-grown pores): (a) top view and (b) oblique view. (c) Optical views of the three SAAO samples with the same pore diameter (30 nm). The variation of the interference colors indicates a difference in the alumina layer thickness (200, 400 and 800 nm). SAAO, sulfuric anodic aluminum oxide; SEM, scanning electron microscopy.

The results of the receding contact angle measurements are not displayed. The receding contact angle measured on the smooth OAAO sample was found to be $(32° \pm 3°)$. All other receding angles (on OAAO or SAAO nanoporous samples) are zero. Actually, in spite of all the care put into making and refining the measurements, the three-phase line never moved backward (never receded). Instead, after all the liquid was pumped back from the droplet, a thin liquid film could be seen remaining on the samples. This film still wet the same area as the original droplet. The contact line was pinned. One sample could be easily used again after it was blown dry with nitrogen for about 10 s.

3.3 Theoretical treatment

3.3.1 Advancing contact angles

Instead of directly plotting the advancing contact angle, as performed in Figure 3, it is better to plot the cosine of this angle because all energy and mechanical relationships are based on cosθ (Cassie, Wenzel and Young). As discussed above, the advancing contact angle is a quantity that depends on the solid structure under the three-phase line. Nevertheless, just like a pure mathematical surface is an idealized physical concept, and must have a thickness, a line must also have a thickness. Choi *et al.* showed that the classical surface-texture parameter is irrelevant in the advancing contact angle description when the hypothetical displacement of the contact line is small compared with the characteristic pitch of the surface.[4] Instead, they recommend that a differential parameter is used. Choi *et al.* worked with surfaces textured on the 100-µm scale. Gao and McCarthy[14] have challenged the validity of the Cassie–Baxter model. This article quickly generated a lot of interest.[15–19] The overall consensus is a widespread vision that reconciles experimental observations and theoretical concepts. The main lesson is that one should consider the *local* values of the surface properties more than the *average* values.[15,16,19] However, in the case of

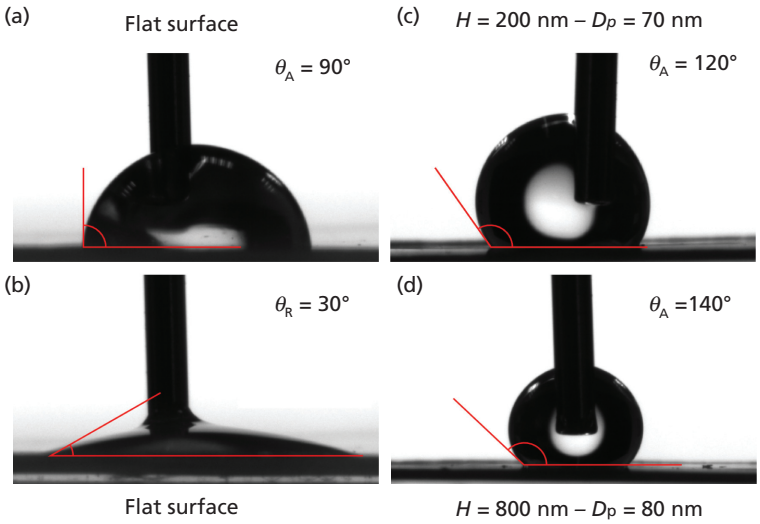

Figure 2. Optical views of the contact angle hysteresis measurement. (a) and (b) Advancing and receding contact angles on the flat OAAO sample. (c) and (d) Advancing contact angles on two OAAO samples. OAAO, oxalic anodic aluminum oxide.

SAAO samples					OAAO samples				
d_p (nm)	20	25	30	40	d_p (nm)	25	50	70	80
θ_A (S200)	96°	100°	106°	119°	θ_A (O200)	102°	113°	125°	138°
θ_A (S400)	95°	100°	106°	120°	θ_A (O400)	106°	114°	133°	138°
θ_A (S800)	96°	102°	105°	120°	θ_A (O800)	100°	117°	130°	140°
$\langle\theta_A\rangle$	95·5°	101°	105·5°	119·5°	$\langle\theta_A\rangle$	103°	115°	129°	139°
$\pm\Delta\theta_A/2$	±0·5°	±1°	±0·5°	±0·5°	$\pm\Delta\theta_A/2$	±3°	±2°	±4°	±1°
					Flat OAAO	θ_A = 90°			

OAAO, oxalic anodic aluminum oxide; SAAO, sulfuric anodic aluminum oxide.

Table 2. Advancing contact angles of water on SAAO and OAAO nanoporous surfaces for different pore depth and radius. The table also displays the mean values, $\langle\theta_A\rangle$, of the Sxxx and Oxxx series for each d_p as well as the observed half deviation, $\Delta\theta_A/2$. The advancing contact angle measured on the flat and smooth OAAO sample is also given.

our nanoporous alumina substrates, the characteristic pitch is likely to be of the order of magnitude of the three-phase line extension, itself, or even lower. The concept of line thickness is more appropriate than a small and 'hypothetical' displacement of the contact line. That is the reason why $\cos\theta_A$ is plotted as a function of Φ_p, the fraction of the pore opening area to the apparent surface area. The surface of a pore opening is $S_p = \frac{\pi}{4} d_p^{\,2}$. The hexagonal cell surrounding this pore opening has a diagonal D, so its surface is $S_{cell} = \frac{\sqrt{3}}{2} D^2$. Fraction Φ_p is then

1. $$\Phi_p = \frac{S_p}{S_{cell}} = \frac{\pi}{2\sqrt{3}} \left(\frac{d_p}{D}\right)^2$$

Φ_p has an areal interpretation, as developed above. θ_A should vary linearly with Φ_p and the trendline should pass through the point ($\Phi_p = 1$, $\cos\theta_A = -1$), to match the Cassie equation applied to the advancing contact angle:

2. $$\cos\theta_{A,Cassie} = (1-\Phi_p)\cos\theta_{A,0} - \Phi_p$$

The left part of Figure 4 shows a top view of the porous surface, with the contact line zone crossing it. On this diagram, the contact line width is greater than d_p and D, supporting the idea that the surface fraction Φ_p is relevant. The plot of $\cos\theta_A$ versus Φ_p is displayed in Figure 5. A linear trend is observed (solid lines). However, several issues remain. First, the acid used for the fabrication, not only sets the distance D between

the pores but also affects the reference advancing contact angle on a flat and smooth surface, $\cos\theta_{A,0}$ (i.e. the two trendlines do not intersect the *y* axis at the same ordinate). Furthermore, in Figure 5, the point of the poreless OAAO sample is not on the OAAO trendline, instead it is closer to the SAAO trendline. The Cassie model is also plotted. The value of $\cos\theta_{A,0}$ used in this model is not set to the value measured on the flat OAAO template, instead it is set to the ordinate of the intersection of each trendline with the vertical axis. This prevents the Cassie model from being too different from the experimental trends. However, even with this stipulation, the trendlines of the two series are still far from the Cassie model prediction. The slopes of the lines are displayed on the graph. They differ too much to be explained by the small uncertainties in the experimental data. In the case of SAAO, the slopes differ by 52% (1·0–1·52) although the difference is less in the case of OAAO, 20% (0·83–1·0).

This last result indicates that a surface approach of the three-phase line advancing criterion is not satisfactory, even with pores as small as 20 nm in diameter spaced 65 nm apart (SAAO). Next, the authors apply the linear approach to the contact line, which is the equivalent of Choi's differential parameter:

$$\cos\theta_{A,linear} = (1-\varphi_p)\cos\theta_{A,0} - \varphi_p \quad (3.)$$

where φ_p is the ratio of the length of contact with a pore opening to a given contact line length ($\varphi_p \propto \sqrt{\Phi_p}$). $\cos\theta_A$ is expected to be as low as possible. The situation that fulfils this constraint is when the contact line crosses a pore opening through its diameter d_p. In this case, φ_p is maximum and takes a value of d_p/D. Plotting $\cos\theta_A$ against d_p/D will indicate whether this linear equation holds. This is shown in Figure 6. The right part of Figure 4 depicts a situation where the contact line thickness is much lower than d_p, supporting the idea that a line-fraction, φ_p, is relevant. These results are encouraging. Linear trends are still observed for both the SAAO and OAAO series. Again, this plot indicates that the wetting of the alumina is different for the different anodization electrolytes. This should not be surprising because it is known that the acid anion of the electrolyte (oxalate and sulfate here) are present in the anodized layer.[20–22] This difference in the oxide composition is probably sufficient to change the surface energy and hence contact angles. The fits shown in Figure 6 are encouraging. First, the result of the flat OAAO sample is consistent with the rest of the nanoporous OAAO samples (the point is on the trendline). Second, the trendlines of the two series both pass through the point ($\cos\theta_A = -1$; $\varphi_p = 1$). This latter result is consistent with the fact that the hypothetical width of the contact line is much lower than the smallest diameter of the samples used (20 nm).

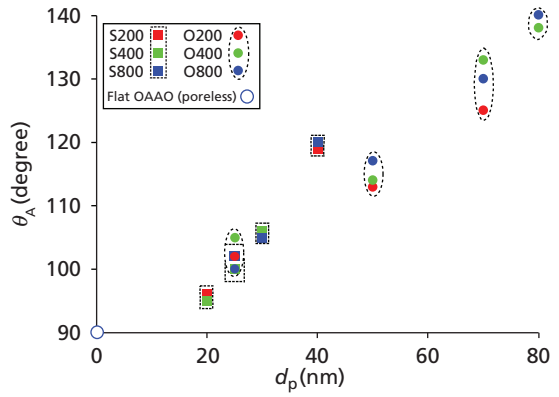

Figure 3. Advancing contact angles plotted as a function of the pore diameter, d_p. For clarity, the points of the Sxxx (Oxxx) series are framed for each diameter.

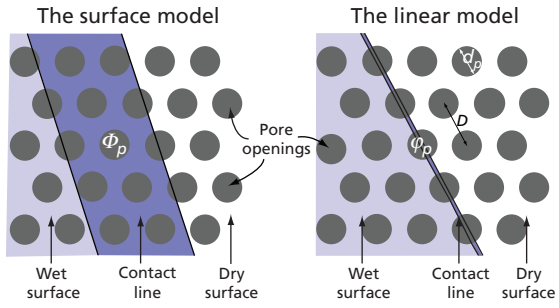

Figure 4. Diagrams of the top view of a nanoporous surface crossed by a liquid–solid contact line (the droplet edge). Left: case of a wide line covering several pore openings. The surface ratio Φ_p is used in the surface model. Right: case of a thin line crossing the pore openings. The linear ratio φ_p is used in the linear model.

3.3.2 Receding contact angles

The results obtained for the receding contact angles (they are always zero) are not so easy to interpret. If we assume the process is reversible (we know it is not but it is a starting point), then the pores filled by the liquid during the wetting step can be emptied. In these conditions, the direction of the contact line that ensures the lowest contact angle is between two parallel rows of pores. So, $\varphi_p = 0$ and θ_R should be around $\theta_{R,0}$, the smooth alumina receding contact angle (32° on oxalic surface). The Young contact angle of water on alumina is about 80°. Even though the authors assume this value can change with the chemistry of the alumina layer, it definitely does not explain these observations.

Another possibility is that the contact line leaves filled pores behind when it recedes. The authors showed in a previous work[1] that such nanopores are easily filled by liquids. It is supported by the huge Laplace pressure of the liquid inside one pore. The difference between the pressure inside and outside is given by $\Delta P = 4\gamma\cos\theta_Y / d_p$. The pressure inside is, in the most favorable scenario (d_p = 80 nm), about 6 bar. It reaches 24 bar when d_p = 80 nm. This situation is not inconsistent with the linear Cassie–Baxter model used to describe the advancing contact line.

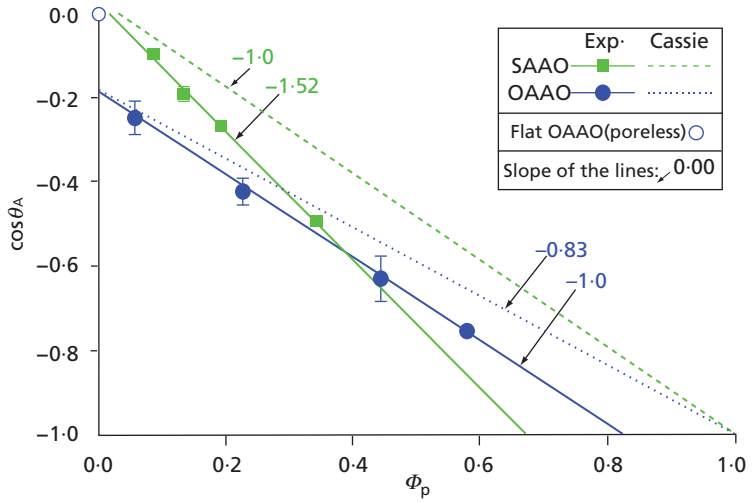

Figure 5. Plot of the experimental advancing contact angles measured for SAAO and OAAO nanoporous samples versus the fraction of pore opening area at the surface, Φ_p. The $\Phi_p = 0$ vertical line corresponds to the smooth surface (poreless sample). The solid lines are the trendlines of each series of points. The dashed lines depict the Cassie model. The slopes are explicitly shown. OAAO, oxalic anodic aluminum oxide; SAAO, sulfuric anodic aluminum oxide.

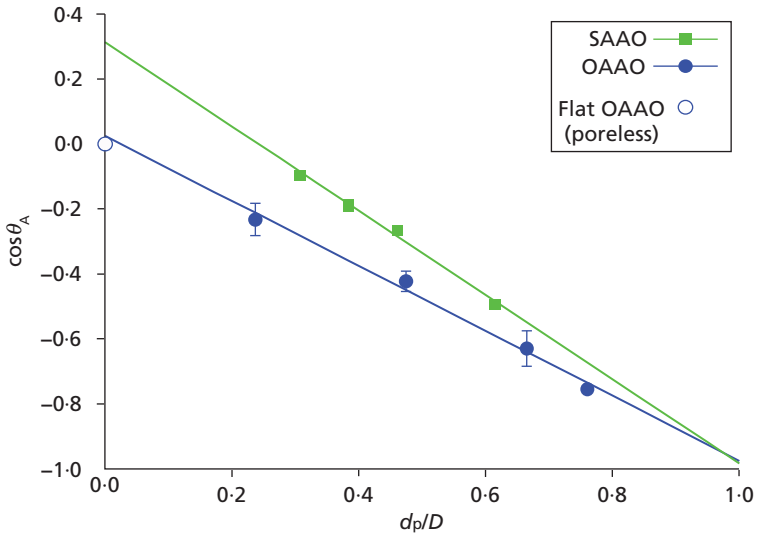

Figure 6. Plot of the experimental advancing contact angles measured with SAAO and OAAO nanoporous samples against the maximum value of the linear ratio φ_p (d_p/D). The left vertical axis ($d_p/D = 0$) corresponds to the smooth surface of a poreless sample. The solid lines are the trendlines for each series. OAAO, oxalic anodic aluminum oxide; SAAO, sulfuric anodic aluminum oxide.

Indeed, this model is definitely expected to apply only to the thin contact line zone. After the contact line has been pushed forward, a liquid meniscus is created on top of the pore which is quickly filled. This means that when the contact line is pulled back, it will tend to jump to a near full-tube opening (without a noticeable macroscopic displacement because of the small pore spacing), so that it is in contact with the water of the pore. The equation describing this is

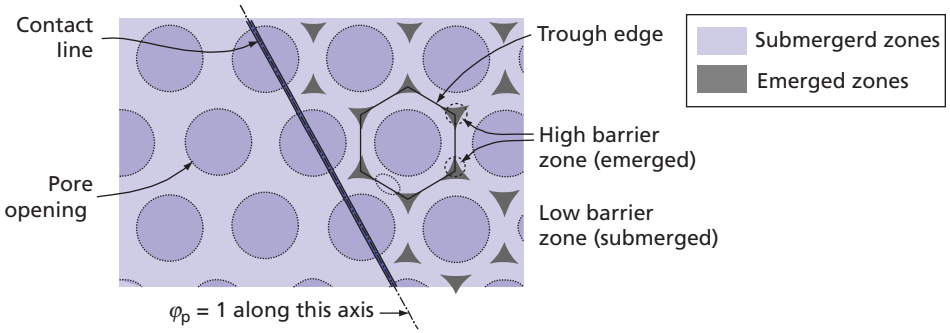

Figure 7. Sketch of the top view of a nanoporous surface. The troughs surrounding each pore may hold water and allow the contact line pinning and $\theta_R = 0$.

4. $$\cos\theta_{R,linear} = (1-\varphi_p)\cos\theta_{R,0} + \varphi_p$$

where φ_p must be maximized to minimize θ_R. We already know this situation, we need $\varphi_p = d_p/D$. One quickly realizes that the only solution where $\theta_{R,linear}$ is with $d_p = D$. This condition is not satisfactory because $d_p < D$ for all the samples studied here.

This description of the nanoporous system may not be accurate enough to fully understand what is going on. The problem lies with the real morphology of the nanoporous surface. The surface surrounding the pore openings is actually not as flat as we assumed up to now. Instead, looking carefully at Figure 1(b) shows that the openings are surrounded by shallow trough-shaped depressions, that is, the barrier around a trough has a variable height. The height at the meeting point of three troughs is maximum. It is minimum between two pores (Figure 7). Again, on the basis of the capillarity considerations, it is imagined that the water inside a trough remains, as it does inside a pore. If the liquid level is higher than the lowest barriers, some parts are submerged. Thus, there exist lines, characterized by $\varphi_p = 1$, and Equation 4 now does hold. The contact line might be pinned along such pore rows and be able to withstand a contact angle equal to zero.

4. Conclusions

In this study, the authors fabricated a set of 24 nanoporous anodic alumina templates, with different morphologies. The distance between the pores, the pore diameter and the pore depth were all varied. A flat, smooth anodic surface was used as a reference. The wettability of these surfaces was studied through the advancing and receding contact angle measurements. The strong hysteresis observed for all the nanoporous surfaces studied is a sign of strong adhesive properties. The advancing angles increase with the pore diameter, irrespective of the distance between the pores, but the angles are not significantly affected by the pore depth. The comparison of these angles with a surface-approach model indicates that the contact line thickness is lower than 20 nm. These conclusions were supported by a linear-approach model indicating the validity of this model down to a 10-nm scale.

Another observation is that the sulfuric- and oxalic-type aluminas have different intrinsic advancing angles. This is probably because the anodization electrolyte affects the chemical composition of the alumina layer, so the sulfuric- and oxalic-type aluminas have different intrinsic advancing angles. Finally, the receding contact angle measurements always gave a value of zero for the receding contact angle. The assumption of the pore-filling irreversibility, due to a large Laplace overpressure, is not sufficient to explain these results. Further analysis of this situation prompted us to consider the surface's shape around the pores. Indeed, the authors found that shallow trough-shaped depressions surrounding the pore openings could remain wet behind the receding contact line. This effect can make entire rows remain wet so that the contact line is pinned along such lines, leading to near-zero receding contact angles.

Acknowledgement

The authors acknowledge the Université d'Auvergne for its financial support and the National Science Foundation funded center C–SPIN, the Oklahoma/Arkansas MRSEC (DMR-0520550).

REFERENCES

1. Raspal, V.; Awitor, K. O.; Massard, C.; Feschet-Chassot, E.; Bokalawela, R. S. P.; Johnson, M. B. Nanoporous surface wetting behavior: the line tension influence. *Langmuir* **2012**, *28*(30), 11064–11071.
2. Miwa, M.; Nakajima, A.; Fujishima, A.; Hashimoto, K.; Watanabe, T. Effects of the surface roughness on sliding angles of water droplets on superhydrophobic surfaces. *Langmuir* **2000**, *16*(13), 5754–5760.
3. Johnson, R. E. Jr.; Dettre, R. H. Contact angle hysteresis. III. Study of an idealized heterogeneous surface. *The Journal of Physical Chemistry* **1964**, *68*(7), 1744–1750.

4. Choi, W.; Tuteja, A.; Mabry, J. M.; Cohen, R. E.; McKinley, G. H. A modified Cassie-Baxter relationship to explain contact angle hysteresis and anisotropy on non-wetting textured surfaces. *Journal of colloid and interface science* **2009**, *339*(1), 208–216.
5. Ramos, S. M. M.; Charlaix, E.; Benyagoub, A. Contact angle hysteresis on nano-structured surfaces. *Surface science* **2003**, *540*(2), 355–362.
6. Ramos, S. M. M.; Charlaix, E.; Benyagoub, A.; Toulemonde, M. Wetting on nanorough surfaces. *Physical Review E* **2003**, *67*(3), 031604.
7. Jeong, H. E.; Kwak, M. K.; Park, C. I.; Suh, K. Y. Wettability of nanoengineered dual-roughness surfaces fabricated by UV-assisted capillary force lithography. *Journal of colloid and interface science* **2009**, *339*(1), 202–207.
8. Kurihara, K.; Suzuki, Y.; Suto, K.; Shiba, N.; Nakano, T.; Tominaga, J. Wettability control using large-area nanostructured film. *Microelectronic Engineering* **2010**, *87*(5–8), 1424–1427.
9. Fan, J. G.; Tang, X. J.; Zhao, Y. P. Water contact angles of vertically aligned Si nanorod arrays. *Nanotechnology* **2004**, *15*, 501.
10. Balaur, E.; Macak, J. M.; Tsuchiya, H.; Schmuki, P. Wetting behaviour of layers of TiO2 nanotubes with different diameters. *Journal of Materials Chemistry* **2005**, *15*(42), 4488–4491.
11. Redon, R.; Vázquez-Olmos, A.; Mata-Zamora, M. E.; Ordóñez-Medrano, A.; Rivera-Torres, F.; Saniger, J. M. Contact angle studies on anodic porous alumina. *Journal of colloid and interface science* **2005**, *287*(2), 664–670.
12. Li, A.; Müller, F.; Birner, A.; Nielsch, K.; Gösele, U. Hexagonal pore arrays with a 50-420 nm interporedistance formed by self-organization in anodic alumina. *Journal of Applied Physics* **1998**, *84*, 6023.
13. Wang, H.; Premachandran Nair, R.; Zou, M.; Larson, P. R.; Pollack, A. L.; Hobbs, K. L.; Johnson, M. B.; Awitor, O. K. Friction study of a Ni nanodot-patterned surface. *Tribology Letters* **2007**, *28*(2), 183–189.
14. Gao, L. C.; McCarthy, T. J. How Wenzel and Cassie were wrong. *Langmuir* **2007**, *23*(7), 3762–3765.
15. McHale, G. Cassie and Wenzel: were they really so wrong? *Langmuir* **2007**, *23*(15), 8200–8205.
16. Panchagnula, M. V.; Vedantam, S. Comment on How Wenzel and Cassie were wrong by Gao and McCarthy. *Langmuir: the ACS journal of surfaces and colloids* **2007**, *23*(26), 13242–13243.
17. Gao, L. C.; McCarthy, T. J. Reply to Comment on How Wenzel and Cassie Were Wrong by Gao and McCarthy. *Langmuir* **2007**, *23*(26), 13243–13243.
18. Erbil, H. Y.; Cansoy, C. E. Range of applicability of the Wenzel and Cassie–Baxter equations for superhydrophobic surfaces. *Langmuir* **2009**, *25*(24), 14135–14145.
19. Nosonovsky, M. On the range of applicability of the Wenzel and Cassie equations. *Langmuir* **2007**, *23*(19), 9919–9920.
20. Sulka, G. D. Highly ordered anodic porous alumina formation by self-organized anodizing. In *Nanostructured Materials in Electrochemistry*. (Eftekhari, A. (ed)). Weinheim: Wiley VCH, 1–116, 2008.
21. Thompson, G. E.; Wood, G. C. Anodic films on aluminum. In *Treatise on Materials Science and Technology, Vol. 23. Corrosion: Aqueous Processed and Passive Films*. (Scullym, J. C. (ed.)). New York: Academic Press, 205–329, 1983.
22. Wernick, S.; Pinner, R.; Sheasby, P. G. Anodizing of aluminium: general notes and theory. In *The Surface Treatment Finishing of Aluminium and Its Alloys*. , 2nd edn. Middlesex: Finishing publications Ltd, 289–368, 1987.

WHAT DO YOU THINK?

To discuss this paper, please email up to 500 words to the managing editor at sufi@icepublishing.com

Your contribution will be forwarded to the author(s) for a reply and, if considered appropriate by the editor-in-chief, will be published as a discussion in a future issue of the journal.

ICE Science journals rely entirely on contributions sent in by professionals, academics and students coming from the field of materials science and engineering. Articles should be within 5000-7000 words long (short communications and opinion articles should be within 2000 words long), with adequate illustrations and references. To access our author guidelines and how to submit your paper, please refer to the journal website at www.icevirtuallibrary.com/sufi